



Article

Magnetic Properties of the Fe₂B Alloy Doped with Transition Metal Elements

Diana Benea * and Viorel Pop

Faculty of Physics, Babeș-Bolyai University Cluj-Napoca, Kogălniceanu Str. 1, 400084 Cluj-Napoca, Romania
* Correspondence: diana.benea@ubbcluj.ro

Abstract: The intrinsic magnetic properties (magnetic moments, magneto-crystalline anisotropy, Curie temperatures) of the (Fe_{1-x}M_x)₂B alloys have been calculated using the spin-polarized relativistic Korringa–Kohn–Rostoker (SPR-KKR) band structure method. The transition metal elements M (M = Co, Ni, Mo, Ta, W and Re) considered in the present study are reported to form stable M₂B or FeMB alloys with a tetragonal Cu₂Al structure type. The experimental studies show that the Fe₂B alloy has a large magnetization (173 Am²/kg), a large Curie temperature (1017 K) and a relatively large anisotropy constant K_1 (-0.80 MJ/m³), but the alloy is inappropriate for permanent magnet applications due to in-plane easy magnetization axis (EMD). The present investigations show the magnetocrystalline anisotropy behaviour by doping with selected d-elements aiming to find an appropriate dopant which is able to switch the EMD from planar to axial and to enhance the magnetocrystalline anisotropy energy (MAE) value without a major decrease of magnetization and Curie temperature.

Keywords: ab initio calculations; magneto-crystalline anisotropy; rare-earth-free magnets

1. Introduction



Citation: Benea, D.; Pop, V. Magnetic Properties of the Fe₂B Alloy Doped with Transition Metal Elements. *Magnetochemistry* **2023**, *9*, 109. <https://doi.org/10.3390/magnetochemistry9040109>

Academic Editor: Cristina Favieres

Received: 31 March 2023

Revised: 13 April 2023

Accepted: 18 April 2023

Published: 20 April 2023



Copyright: © 2023 by the authors. Licensee MDPI, Basel, Switzerland. This article is an open access article distributed under the terms and conditions of the Creative Commons Attribution (CC BY) license (<https://creativecommons.org/licenses/by/4.0/>).

Iron borides have remarkable properties, being part of the steel boriding process widely used in the steel industry. Due to their extreme hardness, brittleness, micro-alloying with iron and chemical inertness, borides are used to increase the hardenability of steel [1]. The FeB and Fe₂B compounds occur as precipitates in amorphous alloys, but they can also be obtained from the high-temperature synthesis route [2]. Studies on the iron borides also reveal their potential use for H storage and fuel cell applications [3,4] or in the magnetically induced hyperthermia [5].

Recent investigations on polycrystals of Fe₂B [6] show their excellent magnetic properties characterized by a large saturation magnetization (173 Am²/kg) and a relatively large magnetic moment per Fe (about 1.9 μ_B). A Curie temperature of 1017 K has been measured for Fe₂B polycrystals [6]. Previous investigations on the magnetic anisotropy of the Fe₂B alloy [7,8] showed a peculiar behaviour with increasing temperature. At a low temperature, the Fe₂B alloy is characterized by an in-plane easy magnetization direction (EMD) which changes the sign, becoming axial with increasing temperature (at 524 K) and reaching a maximum value of ~ 200 kJ/m³ at ~ 750 K [8].

Iron borides are economical and non-toxic raw materials, and by improving their magnetic properties, one could increase their potential use as functional rare-earth-free magnetic materials. To be considered as performant permanent magnets, the materials should have (i) ferromagnetic ordering with a high Curie temperature, (ii) a large saturation magnetization and (iii) a strong magnetic anisotropy of the easy-axis type [9]. As the (i) and (ii) conditions are fulfilled for Fe₂B, a practical route to obtain a rare-earth-free material with an easy-axis anisotropy is to substitute Fe with heavier transition elements, such as 4d or 5d, which have stronger spin-orbit coupling and could support the enhanced easy-axis anisotropy needed for a permanent magnet material [9,10].

As magnetocrystalline anisotropy arises from the spin-orbit coupling, substituting Fe with an $4d/5d$ element such as Mo, Ta, W and Re should increase the magnetocrystalline anisotropy (MAE), as spin-polarized 3d electrons hop into $4d/5d$ orbitals, induce their spin polarization and create large anisotropy due to the large spin-orbit coupling [10]. Another way to increase anisotropy is to create a non-cubic environment by $4d/5d$ element substitution. The 3d dopants could also change the MAE sign of the Fe_2B -based alloys, as the rules to increase the anisotropy are difficult to predict [11]. For example, an axial anisotropy has been found experimentally in $(\text{Fe}_{1-x}\text{Co}_x)_2\text{B}$ alloys for $0.2 \leq x \leq 0.35$ [7].

Theoretical studies on the magnetic properties (total magnetic moments, MAE and Curie temperatures) of $(\text{Fe}_{1-x}\text{M}_x)_2\text{B}$ alloys ($\text{M} = \text{Co}, \text{Ni}, \text{Mo}, \text{W}, \text{Ta}$ and Re) are presented in the following. Our theoretical results are compared with the previous experimental and theoretical data [6,7,9,12] in order to show the reliability of the present study. As suggested by Erdström et al. [12], the coherent potential approximation (CPA) for the substitutional disorder as well as the full potential (FP) approach for the potential symmetry are expected to allow us to give an accurate description for the MAE of the $(\text{Fe}_{1-x}\text{M}_x)_2\text{B}$ alloys. The possibility of obtaining a semihard magnetic alloy with appropriate intrinsic magnetic properties to be integrated in a nanocomposite magnet is discussed.

2. Materials and Methods

The spin-polarized fully relativistic Korringa–Kohn–Rostoker (SPR-KKR) band structure method in full potential mode was used for theoretical calculations [13]. This calculation method is based on the KKR Green's function formalism that makes use of the multiple scattering theory. Within this approach, the scattering properties of each scattering centre (atom) are determined, which are described in the first step by a t -scattering matrix, whereas in the second step, the multiple scattering by all atoms in the lattice is calculated by ensuring that the incident wave at each atom is the sum of the outgoing waves from all other atoms. The central role in the KKR Green's function method is played by the so-called single-particle Green's function, which is efficiently used to determine the crystal Green's function via the Dyson equation. Obviously, the SPR-KKR supplies all the information on the electronic structure, similar to other band structure methods that represent the electronic structure in terms of energy eigenvalues and eigenfunctions. However, using the SPR-KKR band structure method to represent the electronic structure provides the advantage of dealing with chemical disorder, as the coherent potential approximation (CPA) [14] was efficiently integrated [13]. In the coherent potential approximation, the Green's function of an average crystal medium is defined, being determined self-consistently through the condition that the concentration average of the various atom types should not produce any additional scattering in this medium. This is an efficient and reliable method and an alternative to more tedious supercell techniques, which require calculations for several enlarged unit cells with fixed composition followed by the averaging over several atomic configurations in the supercell to describe the alloys properties. More details on the SPR-KKR method are extensively described elsewhere [13].

In the study of the intrinsic magnetic properties of $(\text{Fe}_{1-x}\text{M}_x)_2\text{B}$ alloys, the calculations were performed in the relativistic mode, accounting for all the relativistic effects, including spin-orbit coupling. The angular expansion of the basis set was taken up to $l = 2$ for 3d metal Fe and $l = 3$ for $4d/5d$ metals M. The generalized gradient approximation within the parametrization of Perdew et al. (GGA-PBE) has been used to account for the exchange and correlation effects [15]. The special points method of Monkhorst et al. was used for the k -space integration [16]. Self-consistent band structure calculations have been performed using the full potential approach and the total energy convergence criterion of 10^{-6} Ry.

The study of the magnetic anisotropy was performed using the magnetic torque calculations acting on the magnetic moment \vec{m}_i of the atomic site i , oriented along the magnetization direction \vec{M} [17,18]. The component of the magnetic torque with respect to axis \hat{u} is

$$T_{\hat{u}}(\theta, \varphi) = -\partial E(\vec{M}(\theta, \varphi)) / \partial \theta \quad (1)$$

where θ and φ are the polar angles. The magnetic torque and the energy difference between the in-plane and out-of-plane magnetization directions are related by a special geometry. By setting the angles to $\theta = \pi/4$ and $\varphi = 0$, the calculated magnetic torque is [18]

$$T_{\hat{u}}(\pi/4, 0) = E_{[100]} - E_{[001]} \quad (2)$$

Considering the magnetic anisotropy energy expression by first order approximation $E_a = K_1 \sin^2 \theta$, the magnetic torque $T_{\hat{u}}(\pi/4, 0)$ is equivalent to the anisotropy constant K_1 . A dense k-mesh of $54 \times 54 \times 54$ was used for torque calculations.

The investigation of the magnetic behaviour is based on the classical Heisenberg Hamiltonian described by the expression

$$H_{ex} = - \sum_{ij} J_{ij} \hat{e}_i \cdot \hat{e}_j \quad (3)$$

where the summation is performed on all lattice sites i and j , and \hat{e}_i / \hat{e}_j are the unit vectors of magnetic moments on sites i and j , respectively. The calculations of the J_{ij} exchange-coupling parameters as a function of distance for all magnetic atoms were performed using the expression derived by Liechtenstein [19] based on the magnetic force theorem.

Within Liechtenstein's derivation [19], a total energy difference ΔE_{ij} by an infinitesimal change in the angle between magnetic moments of the (i, j) spin pair is determined. This energy difference is expressed at the lowest order with respect to the angle between \hat{e}_i and \hat{e}_j . A one-to-one mapping between the exchange-coupling energy ΔE_{ij} and the Heisenberg Hamiltonian (3) is obtained, allowing for the expression of the exchange-coupling parameters J_{ij} as [13,19]

$$J_{ij} = -\frac{1}{4\pi} \Im \int_0^{E_F} dE \text{Trace} \left(t_{i\uparrow}^{-1} - t_{i\downarrow}^{-1} \right) \tau_{\uparrow}^{ij} \left(t_{j\uparrow}^{-1} - t_{j\downarrow}^{-1} \right) \tau_{\downarrow}^{ij} \quad (4)$$

Here, $t_{i\uparrow(\downarrow)}^{-1}$ and $\tau_{\uparrow(\downarrow)}^{ij}$ are specific quantities for KKR Green's function method, the first being the spin dependent inverse single-site scattering t -matrices and the second being the scattering path operator which describes all possible scattering events between the sites i and j , respectively.

The Curie temperatures derived using the J_{ij} exchange-coupling parameters within the mean field approach [19,20] have the following expression:

$$T_c^{rough-MFA} = \frac{2}{3k_B} \sum_i J_{0i} \quad (5)$$

where J_{0i} is the exchange-coupling parameters sum over all coordination shells up to 15 Å around lattice site i .

3. Results and Discussions

The Fe₂B alloy crystallizes in the tetragonal Cu₂Al structure type (*I4/mcm* space group) with Fe atoms sitting on *8h* and B atoms on *4a* crystallographic sites. The structure can be seen as alternate layers of Fe and B. The Fe atoms are in a tetragonal surrounding, with two of the Fe–B distances being shorter and the other two being longer than in bcc Fe. The crystal structure of the Fe₂B alloy created using the XCrySDen visualization program [21] is presented in Figure 1.

Previous studies for tetragonal M₂B alloys show a linear lattice constant dependence by the occupation of the *8h* crystallographic site by a binary combination of transitional metal [7,22]. Based on this evidence, the lattice constants used in the theoretical calculations were obtained using the linear dependence of the reported experimental lattice constants [1,7,23–26]. In addition, the experimental free parameter of the *8h* crystallographic site for Fe₂B has been considered [1].

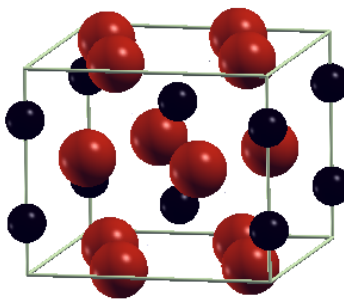


Figure 1. The tetragonal Cu₂Al structure type (*I*4/*mcm* space group) of the Fe₂B alloy, with Fe atoms (red spheres) and B atoms (black spheres).

3.1. Density of States Calculations

The influence of doping on the electronic structure of the (Fe_{1-x}M_x)₂B alloys (M = Co, Ni, Mo, Ta, W and Re) has been investigated using density of states (DOS) calculations (Figure 2). The exchange splitting of total DOS is visible for all (Fe_{1-x}M_x)₂B alloys, suggesting their ferromagnetic order. In order to see the evolution of the DOS by doping with magnetic as well as non-magnetic atoms, the DOS of doped alloys (with M content fixed at x = 0.20) is represented along with that of the undoped Fe₂B alloy. One can notice a different behaviour when the (Fe_{1-x}M_x)₂B alloys are doped with 3d elements (M = Co, Ni) and with 4d/5d-elements (M = Mo, Ta, W, Re). In the 3d doping, the spin-up bands are shifted to the higher energy, diminishing in this way the exchange splitting. On the other hand, the 4d/5d-doping induces a broadening of the electronic bands, which increase from Ta to Re, through an increase of the valence electron numbers. Due to the DOS broadening, the exchange splitting as well as the total magnetic moments of the doped alloys decrease.

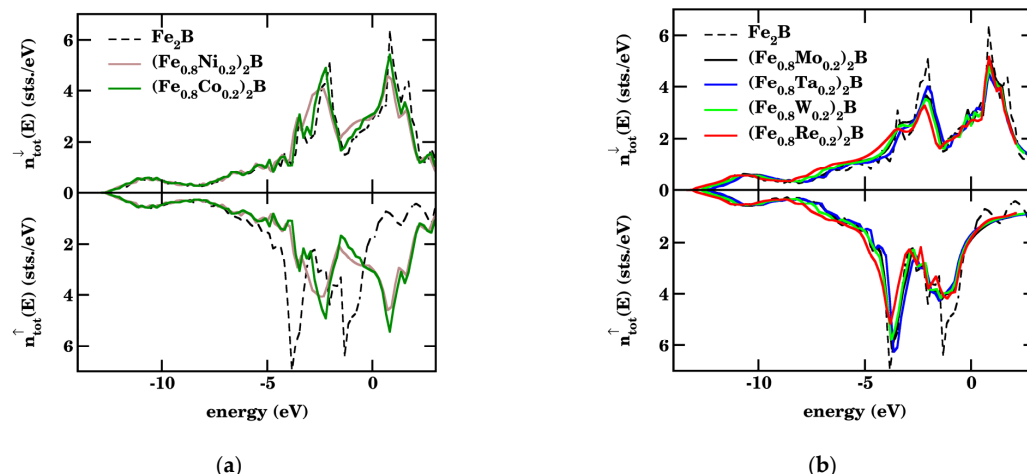


Figure 2. (a) The density of states (DOS) of 3d-doped (Fe_{0.8}M_{0.2})₂B alloys (M = Co, Ni) and (b) the density of states (DOS) of 4d- and 5d-doped (Fe_{0.8}M_{0.2})₂B alloys (M = Mo, Ta, W and Re).

3.2. Magnetic Moments

The band structure calculations for Fe₂B found a spin magnetic moment of $m_s = 3.84 \mu_B/\text{f.u.}$ and an orbital moment of $0.09 \mu_B/\text{f.u.}$ (Table 1). The spontaneous magnetization $\mu_0 M_s$ calculated value is 1.64 T, slightly higher than the value of 1.52 T measured by Coene et al. [27] at room temperature. The calculated mass magnetization is 177.8 Am²/kg, in good agreement with the value determined by Wang et al. (173 Am²/kg) [6]. The spin magnetic moment for Fe atoms is 1.99 μ_B , close to the values obtained by Takacs et al. using Mössbauer spectroscopy at 20 K (1.908 μ_B) [28].

Table 1. Spin and orbital magnetic moments together with the magnetocrystalline anisotropy constant K_1 for the Fe_2B alloy.

Fe_2B	Lattice Const. a, c (Å)	m_s ($\mu_B/\text{f.u.}$)	m_l ($\mu_B/\text{f.u.}$)	$\mu_0 M_s$ (T)	K_1 (meV/f.u.)	K_1 (MJ/m ³)	T_c (K)
Present calc. Exp.	5.11; 4.24 [1]	3.84	0.09	1.64 1.52 [27]	-0.189	-1.09 -0.8 [8]	1284 1017 [6]

The Fe spin (m_s) and orbital (m_l) moments in $(\text{Fe}_{1-x}\text{M}_x)_2\text{B}$ alloys vs. the doping amount x of M elements are represented in Figure 3a,b, respectively. The m_s of Fe ranges between 1.97 and 2.03 μ_B in the investigated doping range (0–0.3). For low doping ($x = 0.04$), all doping elements would induce an increase of the spin magnetic moment of Fe, but this behaviour changes by increasing the doping content. For large doping ($0.12 < x < 0.30$), one can distinguish between the doping elements which reduce the Fe spin moment (Re and Ni) and doping elements which enhance the m_s of Fe ($\text{M} = \text{Co}, \text{W}$ and Mo). The Fe orbital moment (m_l) dependence is almost linear with doping.

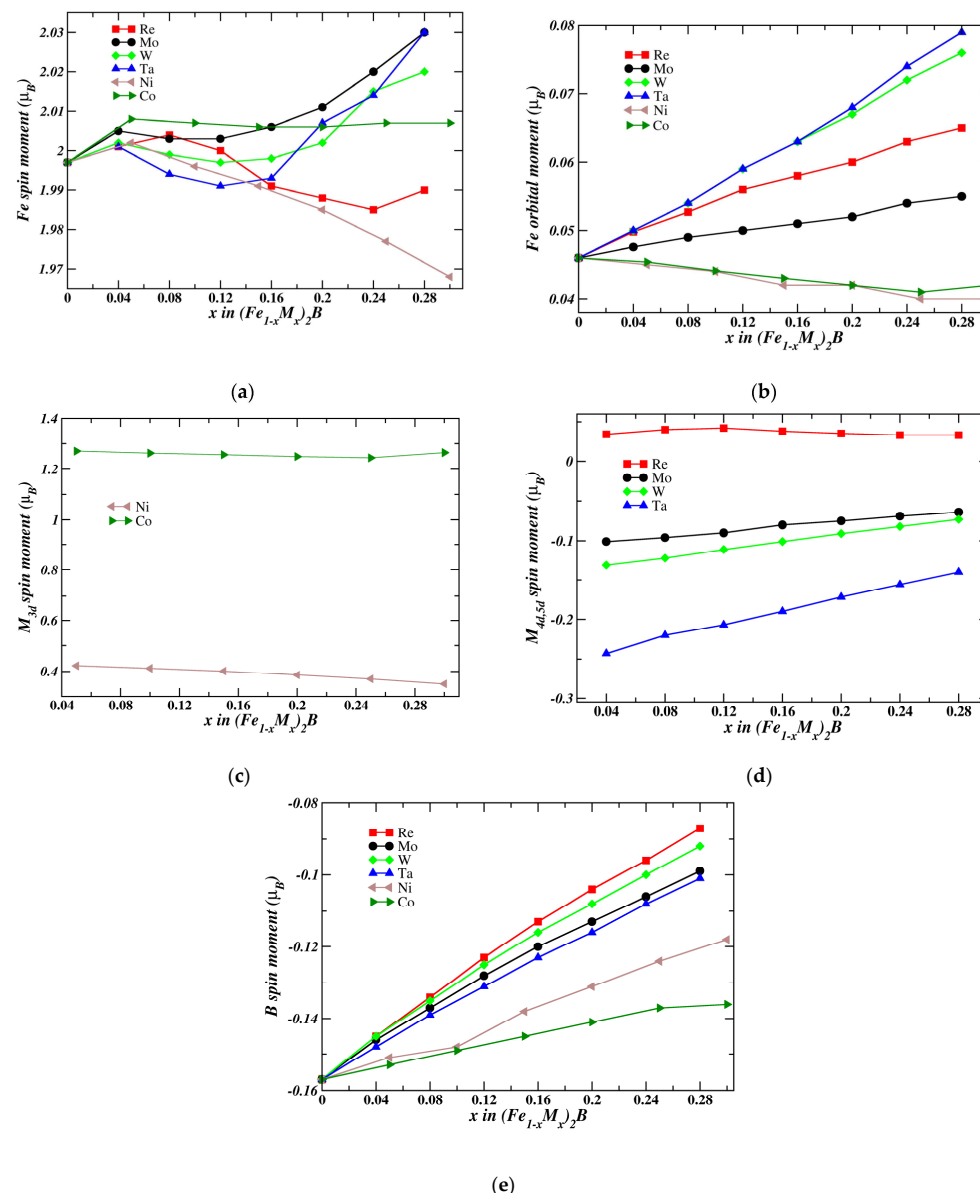


Figure 3. The dependence of the spin and orbital moments of Fe (a,b), M (c,d) and B (e) vs. doping content x in the $(\text{Fe}_{1-x}\text{M}_x)_2\text{B}$ alloys.

Doping with $3d$ elements with smaller spin-orbit coupling reduces the orbital moments of Fe, whereas an increase of m_l is obtained by doping with $4d/5d$ elements, which is more pronounced for $5d$ elements (Ta, W and Re).

The spin magnetic moments of Co and Ni within the $(Fe_{1-x}M_x)_2B$ alloys are represented in Figure 3c vs. the doping amount x . The Co spin moment ($\sim 1.28 \mu_B$) is almost independent of the doping content, whilst the m_s of Ni ranges between 0.42 and $0.38 \mu_B$, decreasing with x . The non-magnetic $4d/5d$ doping elements (Figure 3d) have small induced negative spin moments between -0.1 and $-0.25 \mu_B$ ($M = Ta, W$ and Mo) or small positive induced magnetic moments up to $0.04 \mu_B$ ($M = Re$), slightly dependent on the doping content. The boron spin moment vs. doping content x (Figure 3e) shows its negative polarization, which is reduced by an increase of doping amount x and is more pronounced for $5d$ elements (Re and W) and less pronounced for Co and Ni doping. The M and B orbital moments doping dependencies are negligible and not shown.

The total magnetic moments for $(Fe_{1-x}M_x)_2B$ alloys ($M = Co, Ni, Mo, W, Ta$ and Re) have been used to calculate the magnetization $\mu_0 M_s$, shown in Figure 4. As expected, the $3d$ magnetic elements (Co and Ni) have less impact on the magnetization of $(Fe_{1-x}M_x)_2B$ alloys, but Co is more effective in keeping the large magnetization needed for a permanent magnet. On the other hand, doping with non-magnetic $4d$ and $5d$ elements induces a stronger decrease in magnetization. Between the $4d$ and $5d$ elements, doping with Ta produces a much stronger magnetization decrease compared with Re due to different M-Fe hybridization.

A relatively large value of magnetization is kept by Fe substitutions with $M = Co, Ni$ and partly for Re. Considering the magnetization decrease rate for doping with non-magnetic $4d/5d$ elements, the doping amount was limited ($x \leq 0.28$) for our study, as a further increase of the M content would result in a much lower value of magnetization for permanent magnet applications.

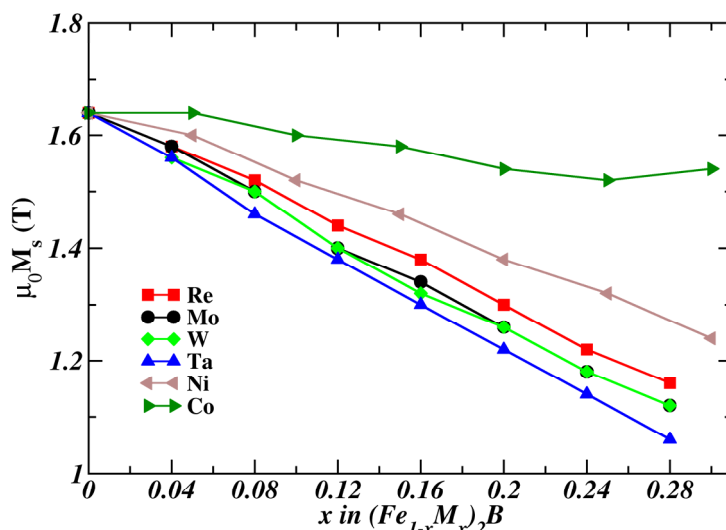


Figure 4. Composition dependence of magnetization $\mu_0 M_s$ in $(Fe_{1-x}M_x)_2B$ alloys ($M = Co, Ni, Mo, W, Ta$ and Re).

3.3. The Magnetocrystalline Anisotropy Energy (MAE)

The magnetocrystalline anisotropy energy $E_{[100]} - E_{[001]}$ for Fe_2B calculated using the torque method is shown in Table 1. As can be seen in Table 1, MAE (K_1) shows an in-plane easy magnetization direction (EMD) with a value of $K_1 = -1.09 \text{ MJ/m}^3$, in agreement with a previous experiment (-0.80 MJ/m^3 [8]).

The calculated values of magnetocrystalline anisotropy (K_1 in kJ/m^3) for the $(Fe_{1-x}M_x)_2B$ alloys ($M = Co, Ni, Mo, W, Ta$ and Re) are shown in Figure 5. As can be seen in Figure 5, the $(Fe_{1-x}M_x)_2B$ alloys have positive anisotropy in a specific doping range only for $M = Co, Re$ and Ta. The case of $(Fe_{1-x}Co_x)_2B$ has been considered extensively by Edström et al. [12].

The theoretical calculations of Edström et al. [12] by Wien2k and FPLO codes using general gradient approximation (GGA) for exchange-correlation potential reproduced the measurements at low temperatures of $K_1(x)$ in $(Fe_{1-x}Co_x)_2B$ very well. The use of coherent potential approximation (CPA) instead of virtual crystal approximation (VCA) removes the MAE overestimation for the Fe-rich alloys. More accurate numerical values of MAE have been obtained using the full potential approach (FP) instead of atomic spheres approximation (ASA) [12].

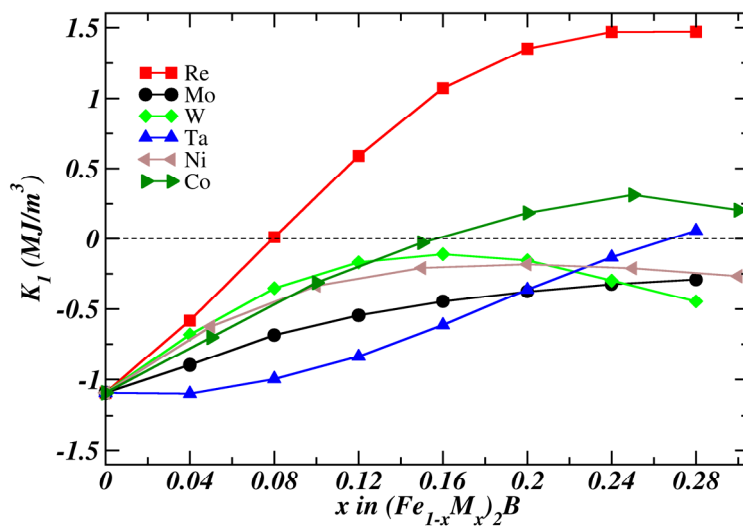


Figure 5. Anisotropy constants K_1 for $(Fe_{1-x}M_x)_2B$ alloys (M = Co, Ni, Mo, W, Ta and Re).

One should note the almost similar behaviour of MAE in $(Fe_{1-x}Co_x)_2B$ alloys obtained in our calculations, with the same interval for the Co amount with positive MAE. The maximum value of K_1 of 0.315 MJ/m^3 for $x = 0.24$ is slightly lower than the anisotropy constant K_1 at room temperature which was obtained for $x = 0.25$ ($K_1 = 450 \text{ kJ/m}^3$) [7]. On the other hand, the theoretical calculations of Edström et al. [12] found $K_1 = 0.77 \text{ MJ/m}^3$ for $x = 0.3$, whilst the experimental K_1 value in the low temperature limit is 0.51 MJ/m^3 for $x = 0.3$ [9]. The numerical differences can be attributed to the different methods used for obtaining the lattice parameters, based on experimental parameters in the present work and by theoretical lattice relaxation [12]. On the other hand, the structural relaxation effects were found to be less effective in the case of Fe ferromagnetic alloys with only $\sim 0.5\%$ reduction of MAE [29].

The most effective substitution to increase the anisotropy in $(Fe_{1-x}M_x)_2B$ alloys is by M = Re with K_1 exceeding 1.2 MJ/m^3 for $x \geq 0.16$. The largest value of K_1 has been obtained for the $(Fe_{0.76}Re_{0.24})_2B$ alloy (1.5 MJ/m^3). A small positive K_1 is obtained for Ta at $x \geq 0.28$, but the Ta doping is less effective for the purpose of the present study, due to an already reduced magnetization value.

Despite their relatively large spin-orbit coupling, negative values of K_1 were found for the other 5d and 4d elements considered in the present study (M = Mo, Ta and W). One should mention the $(Fe_{1-x}Ni_x)_2B$ alloys which have an increased K_1 close to that for M = W, despite the much lower spin-orbit coupling of M = Ni. Other influences on magnetocrystalline anisotropy except spin-orbit coupling might be effective in the case of $(Fe_{1-x}Ni_x)_2B$ alloys, for example, d-band filling or crystal field altering [11].

The disorder effects on the magnetocrystalline anisotropy of an undoped Fe_2B alloy as well as in a Re-doped alloy ($x = 0.12$) with a positive value of K_1 have been investigated. The calculations of K_1 performed for Fe_2B considered a mixing amount δ between the Fe atoms sitting on 8h and B atoms on 4a crystallographic sites, according to the formula $(Fe_{1-\delta}B_\delta)_{2h}^{8h}(B_{1-2\delta}Fe_{2\delta})_{4a}^{4a}$. The K_1 dependence on the intermixing of Fe/B atoms in Fe_2B is shown in Figure 6a. As can be seen in Figure 6a, the disorder effects on the anisotropy constant K_1 of Fe_2B are significant, as an amount of mixing of $\delta = 0.05$ would decrease the

absolute value of anisotropy from -0.19 meV/f.u. to -0.12 meV/f.u. A similar investigation has been performed for the $(\text{Fe}_{0.88}\text{Re}_{0.12})_2\text{B}$ system, considering the intermixing of Re/B atoms (Figure 6b) described by the formula $(\text{Fe}_{0.88}\text{Re}_{0.12-\delta}\text{B}_\delta)_2^{8h}(\text{B}_{1-2\delta}\text{Re}_{2\delta})^{4a}$. The anisotropy constant K_1 of $(\text{Fe}_{0.88}\text{Re}_{0.12})_2\text{B}$ (0.105 meV/f.u. for $\delta = 0$) decreased at zero for $\delta \sim 0.04$, becoming negative for $\delta > 0.04$ with a rate of decrease of ~ 0.02 meV/f.u. per δ mixing amount, which is detrimental for the purpose of reaching a large axial anisotropy in $(\text{Fe}_{1-x}\text{Re}_x)_2\text{B}$ alloys. The mixing of Fe/B atoms between the $8h$ and $4a$ crystallographic sites as well as the mixing of Re/B atoms between the same crystallographic sites are not energetically favourable, as was found by the total energy calculations. Substitutional disorder could occur in the experiment during the preparation (by rapid quenching) or by thermic activation. In the case of the Fe_2B alloy, disorder effects could explain the differences in the K_1 values obtained in the experimental investigations.

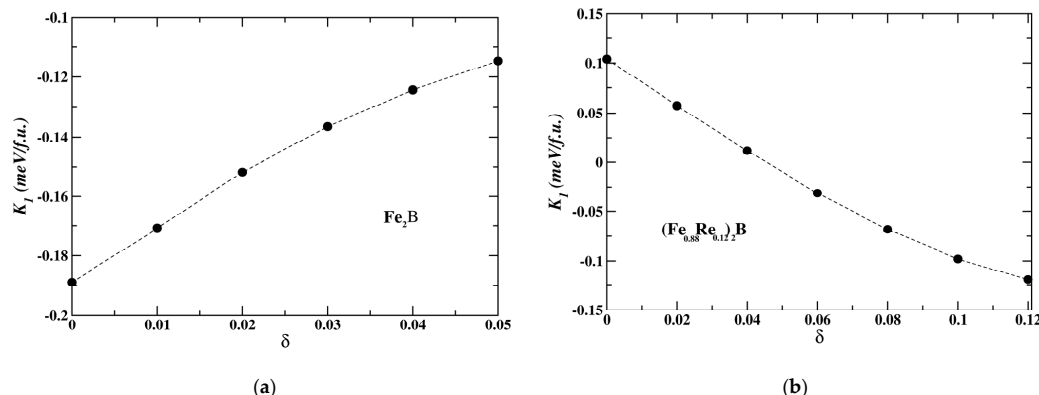


Figure 6. (a) Disorder effects on anisotropy constant K_1 of the Fe_2B alloy. (b) Disorder effects on anisotropy constant K_1 of $(\text{Fe}_{0.88}\text{Re}_{0.12})_2\text{B}$ alloys. Mixing of δ atoms of Fe/B and Re/B has been considered between $8h$ and $4a$ crystallographic sites, respectively.

3.4. The Curie Temperatures

The Curie temperatures calculated using the mean field approach (MFA) for the $(\text{Fe}_{1-x}\text{M}_x)_2\text{B}$ alloys ($\text{M} = \text{Co}, \text{Ni}, \text{Mo}, \text{W}, \text{Ta}$ and Re) are shown in Figure 7. The Curie temperature calculated using the mean field approach (MFA) for Fe_2B gives a value of 1284 K, which is about 20% higher than the experimental value of 1017 K [6]. Knowing this deficiency of the MFA [30], we used also a more realistic estimated Curie temperature, calculated as $T_c^{\text{estim}} = 0.8T_c$, to discuss the T_c behaviour of the alloys with different M doping.

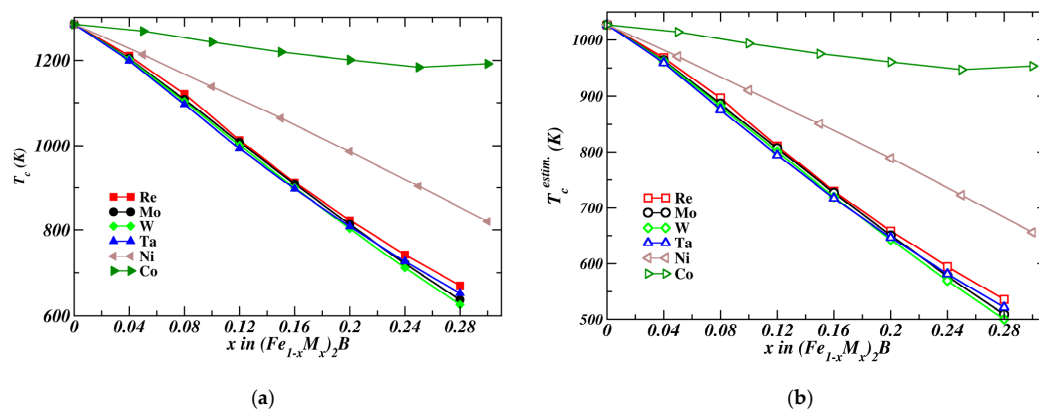


Figure 7. (a) The mean field approach (MFA) calculated Curie temperatures for the $(\text{Fe}_{1-x}\text{M}_x)_2\text{B}$ alloys ($\text{M} = \text{Co}, \text{Ni}, \text{Mo}, \text{W}, \text{Ta}$ and Re) and (b) the estimated Curie temperatures as $T_c^{\text{estim}} = 0.8T_c$.

As can be seen in Figure 7, the largest values of T_c were obtained for the $3d$ magnetic elements; $\text{M} = \text{Co}$, with estimated Curie temperatures over 950 K over the whole doping

range $x \leq 0.3$. For Ni, $T_c^{estim} \geq 650$ K for $x \leq 0.3$. The Curie temperature for M = Re, despite its steep decrease with x content of Re, keeps a $T_c^{estim} \geq 530$ K for $x = 0.28$. The alloy with the highest anisotropy constant K_1 (1.5 MJ/m³) is (Fe_{0.76}Re_{0.24})₂B, which has a magnetization $\mu_0 M_s = 1.22$ T and an estimated Curie temperature $T_c^{estim} = 595$ K, compatible with operating at temperatures under ~250 °C. The calculated hardness parameter for the (Fe_{0.76}Re_{0.24})₂B alloy is $\kappa = 1.1$, slightly beyond the limit for hard magnets [10]. A higher $\mu_0 M_s$ and Curie temperature but lower anisotropy constant K_1 were obtained for the (Fe_{0.8}Re_{0.2})₂B alloy ($\mu_0 M_s = 1.3$ T, MAE of 1.35 MJ/m³, hardness parameter $\kappa = 1.01$, $T_c^{estim} = 660$ K), which would make it suitable for permanent magnet applications. Unfortunately, the relatively large amount of expensive Re is prohibiting the production of such magnetic material on a large scale.

4. Conclusions

Theoretical studies of Fe₂B through doping with selected transition elements M = Co, Ni, Mo, W, Ta and Re show a decrease in the total magnetic moment and Curie temperatures of the alloys by increasing the doping amount, which is more pronounced for non-magnetic 4d/5d elements. The evolution of the anisotropy constant K_1 from planar for the Fe₂B alloy to axial was found only for M = Re, Co and Ta in the investigated doping range ($x \leq 0.28$). The largest theoretical value of the anisotropy constant within the investigated alloys was obtained for (Fe_{0.76}Re_{0.24})₂B with $K_1 = 1.5$ MJ/m³, which is characterized by a magnetization $\mu_0 M_s = 1.22$ T and an estimated Curie temperature $T_c^{estim} = 595$ K. The intrinsic properties of (Fe_{1-x}Re_x)₂B alloys with $x = 0.2\text{--}0.24$ are compatible with those of semihard alloys; these are recommended for further experimental investigations. On the other hand, disorder effects have a strong influence on the MAE of the Fe₂B-based alloys, which must be accounted for by experimental investigations.

Author Contributions: Conceptualization, D.B. and V.P.; methodology, D.B.; software, D.B.; validation, D.B. and V.P.; formal analysis, D.B. and V.P.; investigation, D.B.; resources, D.B.; data curation, D.B.; writing—original draft preparation, D.B.; writing—review and editing, D.B. and V.P.; visualization, D.B.; supervision, D.B. and V.P.; project administration, D.B.; funding acquisition, D.B. All authors have read and agreed to the published version of the manuscript.

Funding: This research was funded by the Romanian Ministry of Education and the Romanian Ministry of Research and Innovation, CCCDI-UEFISCDI grant PN-III-P2-2.1-PED-2019-3484.

Data Availability Statement: No new data were created or analyzed in this study. Data sharing is not applicable to this article.

Conflicts of Interest: The authors declare no conflict of interest. The funders had no role in the design of the study; in the collection, analyses, or interpretation of data; in the writing of the manuscript; or in the decision to publish the results.

References

1. Kapfenberger, C.; Albert, B.; Pöttgen, R.; Huppertz, H. Structure refinements of iron borides Fe₂B and FeB. *Z. Kristallogr.* **2006**, *221*, 477–481. [[CrossRef](#)]
2. Aronsson, B. Borides Part A: Basic Factors. In *Modern Materials*; Hausner, H.H., Ed.; Elsevier: Amsterdam, The Netherlands, 1960; Volume 2, pp. 143–190. [[CrossRef](#)]
3. Umegaki, T.; Yan, J.; Zhang, X.; Shioyama, H.; Kuriyama, N.; Xu, Q. Preparation and catalysis of poly(N-vinyl-2-pyrrolidone) (PVP) stabilized nickel catalyst for hydrolytic dehydrogenation of ammonia borane. *Int. J. Hydrogen Energy* **2009**, *34*, 3816–3822. [[CrossRef](#)]
4. Abrenica, G.H.A.; Ocon, J.D.; Lee, J. Dip-coating synthesis of high-surface area nanostructured FeB for direct usage as anode in metal/metalloid-air battery. *Curr. Appl. Phys.* **2016**, *16*, 1075–1080. [[CrossRef](#)]
5. Hamayun, M.A.; Abramchuk, M.; Alnasir, H.; Khan, M.; Pak, C.; Lenhert, S.; Ghazanfari, L.; Shatruk, M.; Manzoor, S. Magnetic and magnetothermal studies of iron boride (FeB) nanoparticles. *J. Magn. Magn. Mater.* **2018**, *451*, 407–413. [[CrossRef](#)]
6. Wang, D.; Ma, L.; Li, L.; Xu, X.L.; Guo, Y.B.; Zhao, S.Q. Characterization of Polycrystalline Fe₂B Compound with High Saturation Magnetization. *J. Supercond. Nov. Magn.* **2017**, *31*, 431–435. [[CrossRef](#)]
7. Jian, H.; Skokov, K.P.; Kuz'Min, M.D.; Radulov, I.; Gutfleisch, O. Magnetic Properties of (Fe,Co)₂B Alloys With Easy-Axis Anisotropy. *IEEE Trans. Magn.* **2014**, *50*, 2104504. [[CrossRef](#)]
8. Iga, A.; Tawara, Y.; Yanase, A. Magnetocrystalline Anisotropy of Fe₂B. *J. Phys. Soc. Jpn.* **1966**, *21*, 404. [[CrossRef](#)]

9. Kuz'min, M.D.; Skokov, K.; Jian, H.; Radulov, I.; Gutfleisch, O. Towards high-performance permanent magnets without rare earths. *J. Phys. Condens. Matter* **2014**, *26*, 64205. [[CrossRef](#)]
10. Skomski, R.; Coey, J. Magnetic anisotropy—How much is enough for a permanent magnet? *Scr. Mater.* **2016**, *112*, 3–8. [[CrossRef](#)]
11. Skomski, R.; Kashyap, A.; Solanki, A.; Enders, A.; Sellmyer, D.J. Magnetic anisotropy in itinerant magnets. *J. Appl. Phys.* **2010**, *107*, 09A735. [[CrossRef](#)]
12. Edström, A.; Werwiński, M.; Iușan, D.; Rusz, J.; Eriksson, O.; Skokov, K.P.; Radulov, I.A.; Ener, S.; Kuz'Min, M.D.; Hong, J.; et al. Magnetic properties of $(Fe_{1-x}Co_x)_2B$ alloys and the effect of doping by 5 elements. *Phys. Rev. B* **2015**, *92*, 174413. [[CrossRef](#)]
13. Ebert, H.; Ködderitzsch, D.; Minar, J. Calculating condensed matter properties using the KKR-Green's function method—Recent developments and applications. *Rep. Prog. Phys.* **2011**, *74*, 096501. [[CrossRef](#)]
14. Faulkner, J.S.; Stocks, G.M. Calculating properties with the coherent-potential approximation. *Phys. Rev. B* **1980**, *21*, 3222–3244. [[CrossRef](#)]
15. Perdew, J.P.; Burke, K.; Ernzerhof, M. Generalized gradient approximation made simple. *Phys. Rev. Lett.* **1996**, *77*, 3865–3868. [[CrossRef](#)] [[PubMed](#)]
16. Monkhorst, H.J.; Pack, J.D. Special points for Brillouin-zone integrations. *Phys. Rev. B* **1976**, *13*, 5188. [[CrossRef](#)]
17. Staunton, J.B.; Szunyogh, L.; Buruza, A.; Gyorffy, B.L.; Ostanin, S.; Udvardi, L. Temperature dependence of magnetic anisotropy: An *ab initio* approach. *Phys. Rev. B* **2006**, *74*, 144411. [[CrossRef](#)]
18. Mankovsky, S.; Polesya, S.; Bornemann, S.; Minar, J.; Hoffmann, F.; Back, C.; Ebert, H. Spin-orbit coupling effect in (Ga,Mn)As films: Anisotropic exchange interactions and magnetocrystalline anisotropy. *Phys. Rev. B* **2011**, *84*, 201201. [[CrossRef](#)]
19. Liechtenstein, A.; Katsnelson, M.; Antropov, V.; Cubanov, V. Local spin density functional approach to the theory of exchange interactions in ferromagnetic metals and alloys. *J. Magn. Magn. Mater.* **1987**, *67*, 65–74. [[CrossRef](#)]
20. Nieves, P.; Arapan, S.; Maudes-Raedo, J.; Marticorena-Sánchez, R.; Del Brío, N.; Kovacs, A.; Echevarria-Bonet, C.; Salazar, D.; Weischenberg, J.; Zhang, H.; et al. Database of novel magnetic materials for high-performance permanent magnet development. *Comput. Mater. Sci.* **2019**, *168*, 188–202. [[CrossRef](#)]
21. Kokalj, A. XCrySDen—A new program for displaying crystalline structures and electron densities. *J. Mol. Graph. Model.* **1999**, *17*, 176–179. [[CrossRef](#)]
22. Ener, S.; Fries, M.; Hammerath, F.; Opahle, I.; Simon, E.; Fritsch, P.; Wurmehl, S.; Zhang, H.; Gutfleisch, O. Magnetic and magnetocaloric properties of the Co_2-xMn B system by experiment and density functional theory. *Acta Mater.* **2018**, *165*, 270–277. [[CrossRef](#)]
23. Neov, D.; Slavov, L.; Donkov, A.; Mirzayev, M.; Popov, E.; Demir, E.; Siemek, K.; Djourelov, N.; Turchenko, V.; Sharipov, Z.; et al. Structural study of W_2B obtained via mechanical alloying of W, B_4C , TiC and graphite before and after He ions irradiation. *Nucl. Mater. Energy* **2022**, *31*, 101201. [[CrossRef](#)]
24. Havinga, E.; Damsma, H.; Hokkeling, P. Compounds and pseudo-binary alloys with the $CuAl_2(C16)$ -type structure I. Preparation and X-ray results. *J. Less Common Met.* **1972**, *27*, 169–186. [[CrossRef](#)]
25. Akopov, G.; Yeung, M.T.; Kaner, R.B. Rediscovering the Crystal Chemistry of Borides. *Adv. Mater.* **2017**, *29*, 1604506. [[CrossRef](#)] [[PubMed](#)]
26. Villars, P.; Calvert, L.D. *Pearson's Handbook of Crystallographic Data for Intermetallic Phases*, 2nd ed.; ASM international: Novelty, OH, USA, 1991; Volume 3, p. 1615.
27. Coene, W.; Hakkens, F.; Coehoorn, R.; de Mooij, D.; de Waard, C.; Fidler, J.; Grössinger, R. Magnetocrystalline anisotropy of Fe_3B , Fe_2B and $Fe_{1.4}Co_{0.6}B$ as studied by Lorentz electron microscopy, singular point detection and magnetization measurements. *J. Magn. Magn. Mater.* **1991**, *96*, 189–196. [[CrossRef](#)]
28. Takacs, L.; Cadeville, M.C.; Vincze, I. Mossbauer study of the intermetallic compounds $(Fe_{1-x}Co_x)_2B$ and $(Fe_{1-x}Co_x)B$. *J. Phys. F Met. Phys.* **1975**, *5*, 800–811. [[CrossRef](#)]
29. Lawrence, R.A.; Donaldson, S.J.; Probert, M.I.J. Magnetic Transition State Searching: Beyond the Static Ion Approximation. *Magnetochemistry* **2023**, *9*, 42. [[CrossRef](#)]
30. Sato, K.; Bergqvist, L.; Kudrnovsky, J.; Dederichs, P.H.; Eriksson, O.; Turek, I.; Sanyal, B.; Bouzerar, G.; Katayama-Yoshida, H.; Dinh, V.; et al. First-principles theory of dilute magnetic semiconductors. *Rev. Mod. Phys.* **2010**, *82*, 1633–1690. [[CrossRef](#)]

Disclaimer/Publisher's Note: The statements, opinions and data contained in all publications are solely those of the individual author(s) and contributor(s) and not of MDPI and/or the editor(s). MDPI and/or the editor(s) disclaim responsibility for any injury to people or property resulting from any ideas, methods, instructions or products referred to in the content.